Spatial distribution of microwave device harmonic electrical variables through T-dependent TCAD simulations

Spatial distribution of microwave device harmonic electrical variables through T-dependent TCAD simulations

E. Catoggio[#1], S. Donati Guerrieri[#2], F. Bonani[#3], G. Ghione[#4],
[#]Dipartimento di Elettronica e Telecomunicazioni, Politecnico di Torino, Italy
{[1]eva.catoggio, [2]simona.donati, [3]fabrizio.bonani, [4]giovanni.ghione}@polito.it

***Abstract* — TCAD simulations of electron devices operated in the periodic large-signal regime are implemented in the frequency domain, thus allowing extracting all internal physical variables, such as the carrier concentration and electric field, in terms of their harmonic content. Therefore, these simulation tools offer a unique insight into the device operating conditions typical of microwave applications, e.g. highlighting the regions of the device affecting each harmonic of the terminal currents. In particular, Conversion Green's Functions, allow for a simple and direct way to inspect the response of each harmonic to variations in the device operating condition, structure, material and technological parameters with respect to the nominal values. In this paper, we provide a discussion of the internal quantities for a silicon FinFET device, exploited into a power amplifier for small-cells transceiver applications at 70 GHz. The temperature dependent analysis highlights e.g. the impact of carrier mobility degradation in the FinFET access regions and of the inversion channel charge including DC, fundamental and harmonics of the drain current.**

***Keywords* — Semiconductor devices, Nonlinear device models, TCAD simulations, Harmonic Balance**

I. Introduction

Technological CAD (TCAD) simulations in the nonlinear large-signal (LS) regime represent an ideal environment to model the behavior of an active device in RF/microwave circuits, keeping trace of the underlying technological and physical parameters. Nonlinear TCAD analysis dates back to the pioneering work of [1], [2], where the Harmonic Balance (HB) algorithm was introduced to solve the physical equations in the frequency domain. The harmonics of the device solution, in terms of both terminal variables (e.g. drain and gate currents) and internal physical quantities (e.g. electric field, potential and carrier densities) are made directly accessible for the specific device LS operating condition, driven by the external large-signal stimuli. The HB TCAD analysis is perfectly matched to the most common simulation techniques used in microwave circuit simulators (e.g. ADS), making it simple to include in a seamless way the device embedding circuit in terms of harmonic loads, transmission lines, dividers/combiners etc. In [3] the TCAD nonlinear analysis was further extended to represent the device behavior around the LS working point, by a proper linearization of the device equations around a periodic (or quasi-periodic) condition and by an efficient algorithm to extract the Green's Functions of the linearized physical model. Nowadays, the increasing capability of computation machines allows to overcome the numerical burden of nonlinear TCAD analysis making its application possible to investigate realistic devices and structures, even in complex circuits [4].

In this work we focus the attention on the Si FinFET technology, whose application in analog and microwave design is fostered both by the development of modern communication systems (5G/6G), and by the design of sensing circuits for quantum computing. In the latter case, existing FinFET device models face a double problem: first they are not usually tailored for analog application, even less in case of nonlinear ones; secondly, the temperature dependency is usually limited to DC quantities, while it is not simple to predict its effect on harmonics. Last but not least, quantum applications are nowadays mostly found at cryogenic temperatures, making T-dependent physically sound LS FinFET models an important and timely research topic. Our in-house TCAD code [3], allowing for the Harmonic Balance T-dependent Large Signal analysis of electron devices, is the ideal tool to investigate the effect of temperature on FinFET nonlinear operation. In [5] we have demonstrated the temperature sensitivity of the device LS state can be effectively treated as a particular case of the large-signal sensitivity analysis [6], [7], where the variations of the device terminal characteristics (namely, gate and drain currents) are calculated as a function of the variation of any physical or geometrical parameter, such as doping, gate length or trap density. The sensitivity analysis is best addressed by the Green's Function (GF) approach, where the variations terminal currents are recovered by a convolution of a *microscopic source of variation* and of the GFs themselves. As such, the analysis allows to inspect which parts of the device are most affected by the parameter variations or contribute more to the terminal variations. Compared to the static case, also implemented in [8], the LS case addresses the variations not only of the DC current values, but of all of the terminal current harmonics.

In this work we apply the TCAD distributed thermal analysis to the study of a FinFET device operating in nonlinear condition within a Power Amplifier (PA) for small cells applications. This work extends previous published papers on FinFET modeling [9] and PA thermal sensitivity [5], [10]: while previous works have mainly focused on the PA performance in terms of output power, gain, efficiency and terminal currents in the time domain, in this work we report

the temperature dependency of the harmonics and link them to internal portrait of the microscopic quantities in terms of Green's Functions and local variations of physical quantities due to temperature variations. We demonstrate that gate and drain harmonics as a function of input power have peculiar dependencies on temperature, linked to the source and drain access region (e.g. the real part of the 3rd harmonic drain current) or to the channel charge (e.g. the imaginary part of the 3rd harmonic drain current). The distributed analysis opens the way to device optimization, aiming directly to the device harmonics and power performance.

II. Green's Function Technique for T-dependent LS TCAD

In order to introduce the efficient T-dependent TCAD analysis methodology along the lines discussed in [5], let us consider a bipolar physical model, that for TCAD is almost invariably made of a set of coupled partial differential equations (PDEs). For the sake of generality, we consider Poisson equation (referred to by index $\alpha = \varphi$) coupled to the electron ($\alpha = n$) and hole ($\alpha = p$) continuity equations, to the energy balance equations ($\alpha = T_n$ and $\alpha = T_p$, respectively) involving as variables carrier temperatures T_n and T_p, and to the electron and hole quantum potential equations ($\alpha = q_n$ and $\alpha = q_p$) in case quantum corrections such as the density gradient approach are taken into account. Once spatially discretized over device volume Ω after the definition of a proper solution mesh, PDE α is converted into a nonlinear ordinary differential equation (ODE) and it is formally denoted as $\mathbf{E}^{(\alpha)}(\mathbf{x}, \dot{\mathbf{x}}) = \mathbf{0}$, where $\mathbf{x}$ collects the nodal values of all the (discretized) physical variables (i.e., potential φ, carrier concentrations n and p, carrier temperatures T_n and T_p, quantum potentials q_n and q_p) and $\dot{\mathbf{x}}$ denotes its time derivative. Notice that we assume to have included in the ODE the required (discretized) boundary conditions for each physical equation.

Extracting the time-derivative dependence of the ODEs, and making explicit the external generators (either current or voltage) $\mathbf{e}(t)$ setting the device working point, yields the ODE system

$$\mathbf{D}^{(\alpha)}\dot{\mathbf{x}} = \mathbf{F}^{(\alpha)}(\mathbf{x}, \mathbf{e}; T) \qquad \alpha = \varphi, n, p, T_n, T_p, q_n, q_p \quad (1)$$

where $\mathbf{D}^{(\alpha)}$ is a diagonal matrix (possibly null, e.g. for Poisson equation where no explicit time derivative appears).

LS operation amounts to consider source generators $\mathbf{e}(t)$ that are time periodic[1], which in turn suggests to exploit a frequency domain technique such as Harmonic Balance [11] to convert (1) into a nonlinear algebraic equation system having as unknowns the harmonic amplitudes of the time-varying variables. A sound implementation requires a trigonometric representation of the Fourier series, as discussed in [1], so that each harmonic amplitude is actually represented by two real values (one for the sine and one for the cosine components).

[1]The extension to quasi-periodic operation is relatively easy, we stick to the strictly periodic case for the sake of notation simplicity.

The involved (truncated) frequency spectrum is limited to a finite upper harmonic N_H, and it entails the (angular) frequencies $n\omega_0$ ($n = 1, \ldots, N_\mathrm{H}$), where ω_0 is the fundamental frequency contained in $\mathbf{e}(t)$, plus DC. The collection of the $2N_\mathrm{H} + 1$ harmonic amplitudes for each of the N elements of $\mathbf{x}(t)$ is collectively denoted by the $N(2N_\mathrm{H} + 1)$ vector $\tilde{\mathbf{x}}$. Fourier transformation of (1) results into

$$\mathbf{D}^{(\alpha)}\boldsymbol{\Omega}_N\tilde{\mathbf{x}} = \tilde{\mathbf{F}}^{(\alpha)}(\tilde{\mathbf{x}}, \tilde{\mathbf{e}}; T) \quad \alpha = \varphi, n, p, T_n, T_p, q_n, q_p \quad (2)$$

where $\boldsymbol{\Omega}_N$ is an N-block diagonal matrix (proportional to ω_0) representing the time derivative operator in the Fourier basis [3].

At nominal temperature T_0, the solution of (2) is denoted as $\tilde{\mathbf{x}}_0$ (corresponding to the time-domain solution $\mathbf{x}_0(t)$). As temperature undergoes a variation $T = T_0 + \Delta T$, the use of the Green's Functions Technique reckons on the assumption of a linear response of the device to the variation ΔT so that a linearization of the model (1) around $(\mathbf{x}_0(t), \mathbf{e}(t), T_0)$ is required. The resulting linear system is periodically time-varying, also termed LPTV. The general description of LPTV systems is well established [3], and amounts to consider a periodic perturbation at frequency ω. The result is a perturbed spectrum made of *sidebands* around each harmonic of the original spectrum, i.e. spectral components concentrated at $m\omega_0 \pm \omega$ where $m = 0, 1, \ldots, N_\mathrm{H}$. As in the case of T-dependent analysis the temperature perturbation is assumed time-invariant, we have $\omega = 0$ and the sidebands collapse on the original frequency spectrum.

Fourier transformation of the LPTV system resulting from the expansion of (1) around the T_0 solution leads to the following frequency-domain system for equationα [5]

$$\tilde{\mathbf{J}}^{(\alpha)}(\tilde{\mathbf{x}}_0, \tilde{\mathbf{e}}; T_0)\Delta\tilde{\mathbf{x}} - \mathbf{D}^{(\alpha)}\boldsymbol{\Omega}_N\Delta\tilde{\mathbf{x}} = \tilde{\mathbf{s}}^{(\alpha)}(\tilde{\mathbf{x}}_0, \tilde{\mathbf{e}}; T_0, \Delta T) \quad (3)$$

where $\Delta\tilde{\mathbf{x}} = \tilde{\mathbf{x}} - \tilde{\mathbf{x}}_0$ represents the variation of the model solution due to ΔT, $\tilde{\mathbf{s}}^{(\alpha)}$ is the corresponding source term, and $\tilde{\mathbf{J}}^{(\alpha)}(\tilde{\mathbf{x}}_0, \tilde{\mathbf{e}}; T_0)$ is the Jacobian of the original model evaluated at T_0. In particular, the Jacobian takes the form of a Hankel matrix built starting from the harmonic amplitudes (in trigonometric form) of the time-periodic functions corresponding to the time-domain Jacobian $\partial\mathbf{F}^{(\alpha)}/\partial\mathbf{x}$ evaluated in $\mathbf{x}_0(t)$ and at the nominal temperature T_0. On the other hand, the source term $\tilde{\mathbf{s}}^{(\alpha)}$ collects the Fourier coefficients of the temperature model derivative

$$\mathbf{s}^{(\alpha)}(t) = -\left.\frac{\partial\mathbf{F}^{(\alpha)}}{\partial T}\right|_{\mathbf{x}_0(t), \mathbf{e}(t); T_0} \Delta T \quad (4)$$

This quantity can be very conveniently approximated through a finite difference approximation [6] as

$$\mathbf{s}^{(\alpha)}(t) \approx -\mathbf{F}^{(\alpha)}(\mathbf{x}_0(t), \mathbf{e}(t); T_0 + \Delta T) + \mathbf{F}^{(\alpha)}(\mathbf{x}_0(t), \mathbf{e}(t); T_0) \quad (5)$$

where, at convergence, we can assume $\mathbf{F}^{(\alpha)}(\mathbf{x}_0(t), \mathbf{e}(t); T_0) = \mathbf{0}$ so that

$$\mathbf{s}^{(\alpha)}(t) \approx -\mathbf{F}^{(\alpha)}(\mathbf{x}_0(t), \mathbf{e}(t); T_0 + \Delta T) \quad (6)$$

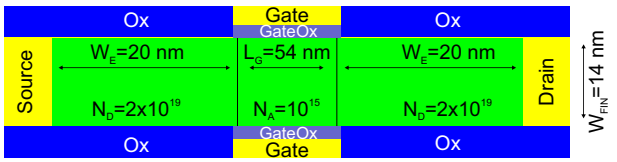

Fig. 1. Double Gate structure representing the cross-section of each elementary fin of the power cell.

The frequency transformation procedure leading to (3) allows to verify that the previous relation can be extended to

$$\tilde{\mathbf{s}}^{(\alpha)} \approx -\tilde{\mathbf{F}}^{(\alpha)}(\tilde{\mathbf{x}}_0, \tilde{\mathbf{e}}; T_0 + \Delta T) \tag{7}$$

This means that also the source term in the frequency domain can be simply estimated by computing the residual part of the nonlinear function in (2) at the updated temperature $T_0 + \Delta T$.

The effect of the temperature variation ΔT on the current harmonic amplitudes $\tilde{\mathbf{I}}_\beta$ at terminal $\beta = \mathrm{G}, \mathrm{D}$, defined as

$$\Delta\tilde{\mathbf{I}}_\beta = \tilde{\mathbf{I}}_\beta(T_0 + \Delta T) - \tilde{\mathbf{I}}_\beta(T_0) \tag{8}$$

can be estimated through a spatial convolution integral across the device volume Ω of the product of the (matrix) Green's function $\tilde{\mathbf{G}}_\beta^{(\alpha)}(\tilde{\mathbf{x}}_0, \mathbf{e}; T_0)$, linking a unit (delta function) source term in equation α to the output current at terminal β, times the source term in (7). Notice that the matrix nature of the Green's function accounts, through the non-diagonal terms as a function of the harmonic index, for the presence of frequency conversion mechanisms (i.e., the impact of a source term at harmonic i on the terminal β current variation at harmonic j, for $i \neq j$). For this reason, these tensor operators are also called *conversion* Green's functions.

The discretized implementation of the spatial convolution integral leads to a final expression of the form [5]

$$\Delta\tilde{\mathbf{I}}_\beta = \sum_\alpha \boldsymbol{\Omega}_\mathrm{V} \tilde{\mathbf{G}}_\beta^{(\alpha)}(\tilde{\mathbf{x}}_0, \mathbf{e}; T_0) \tilde{\mathbf{s}}^{(\alpha)}(\tilde{\mathbf{x}}_0, \mathbf{e}; T_0, T_0 + \Delta T) \tag{9}$$

where $\boldsymbol{\Omega}_\mathrm{V}$ is a block diagonal matrix containing the size of the Vornoi volumes associated to the discretization mesh. Notice that the matrix nature of the conversion Green's functions in (9) leads to the presence of frequency conversion effects, as the matrix-vector products effectively become sums over the frequency index of all the harmonic source components.

The computational cost of a temperature dependent device analysis including N temperatures distributed around T_0 amounts in the evaluation of the GF and N repeated computation of (7) and (9). All these steps require minimal additional simulation time with respect to a single Large Signal analysis at temperature T_0. Therefore the GF approach simulation time is roughly $1/N$ with respect to N independent Large Signal analyses at the selected temperatures.

III. Example: A distributed thermal analysis of a FinFET power amplifier

As a test case we exploit a class A power amplifier for small cells applications based on FinFET technology, with the same topology presented in [5]. A unit cell made of a multi-finger device (10 fingers of 30 fins each) with a fin height of 25 nm, corresponding to a total gate periphery of 15 μm, is used for the development of the power stage. The cross-section of each elementary fin of the power cell is represented in Fig. 1. The device is simulated in large-signal conditions at an operating frequency of 70 GHz. The DC bias ($V_\mathrm{G} = 0.675$ V and $V_\mathrm{D} = 0.6$ V) and the optimum output load $Z_\mathrm{opt} = (53 + \mathrm{j}6)\ \Omega$, calculated at the nominal "cold" temperature $T_0 = 300$, are applied to the device. The input port is unmatched and terminated over a generator internal impedance of 50 Ω/mm. LS simulations, exploiting the in-house Harmonic Balance code, are performed with $N_\mathrm{H} = 10$ harmonics and as a function of an increasing input power ranging from back-off to 2 dB gain compression. At each input power, the Conversion Green's Functions are calculated at $T_0 = 300$ K, while the drain current variation with T is evaluated according to (9) for 5 temperatures, spanning the interval $[310 - 350]$ K.

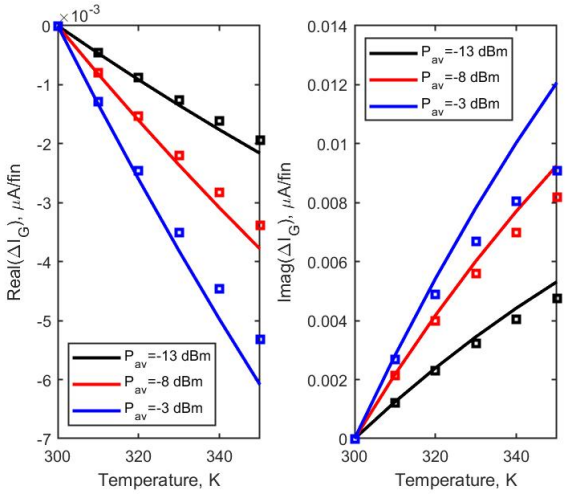

Fig. 2. Real and imaginary part of the fundamental harmonic gate current variation as a function of temperature. Lines: INC approach. Symbols: GF approach.

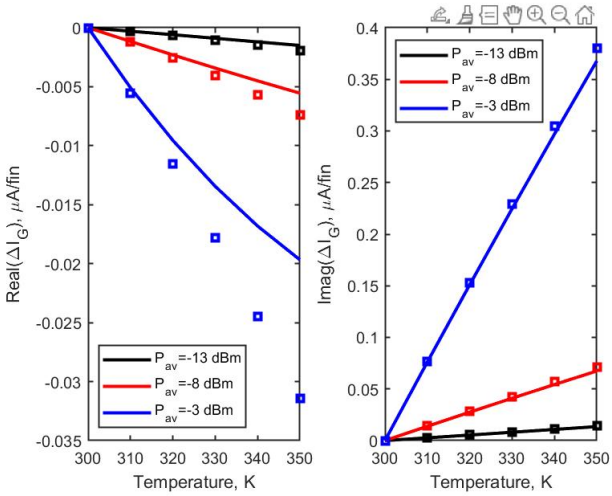

Fig. 3. Real and imaginary part of the second harmonic gate current variation as a function of temperature. Lines: INC approach. Symbols: GF approach.

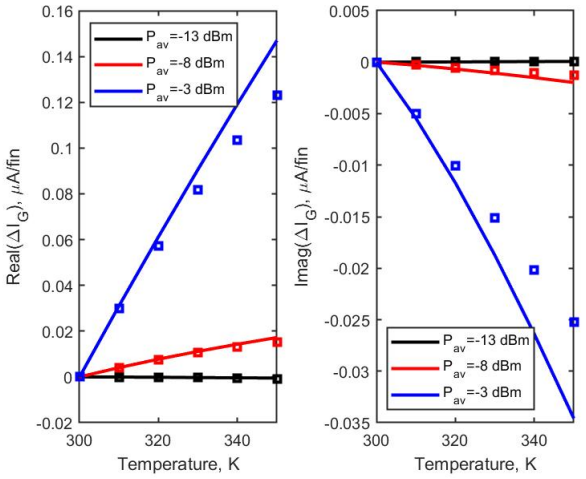

Fig. 4. Real and imaginary part of the third harmonic gate current variation as a function of temperature. Lines: INC approach. Symbols: GF approach.

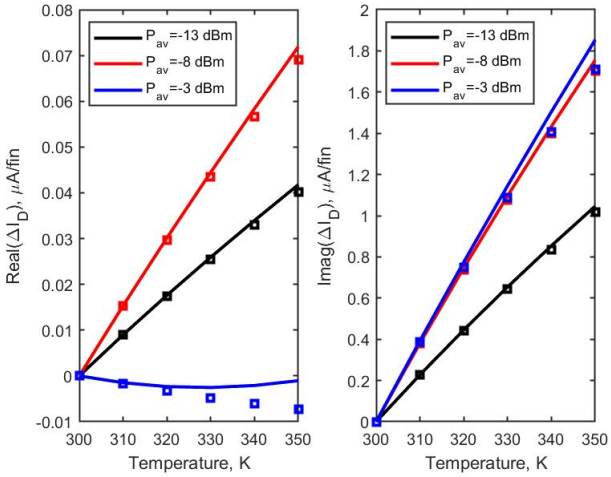

Fig. 5. Real and imaginary part of the first harmonic drain current variation as a function of temperature. Lines: INC approach. Symbols: GF approach.

Fig. 2 shows the gate current variation at the fundamental harmonic as a function of temperature at increasing input power from -13 dBm to -3 dBm. We remark that gate current harmonics are well reproduced by the Green's Function (GF) approach, despite the simulation time is less than 20% of the incremental (INC) method, which consists of repeated LS analyses at 5 different temperatures. An increasing sensitivity can be appreciated going from back-off ($P_{\text{av}} = -13$ dBm) to compression ($P_{\text{av}} = -3$ dBm) in both real and imaginary parts, leading to negative and positive current variations, respectively.

The gate current second harmonic in Fig. 3 shows overall a stronger temperature sensitivity, but exhibits the same trend of the fundamental harmonic as a function of the input power.

Despite the real and the imaginary part of the third harmonic show higher sensitivity with an increasing input power, gate current variations assume positive and negative values, respectively, highlighting an opposite behavior with respect to the first and second harmonics. The highest temperature sensitivity is reached at -3 dBm input power.

Concerning the drain current variation, the real part of the fundamental harmonic has higher sensitivity to temperature variations with lower values of the input power, while an almost insensitive behavior is shown in compression conditions (see Fig. 5). On the contrary, drain current variations of the imaginary part are always relevant and exhibit approximately the same sensitivity at -8 and -3 dBm input power.

The second harmonic dependency on T as a function of the input power is reported in Fig. 6: the real part exhibits an overall higher sensitivity with respect to the fundamental drain harmonics, while an opposite behavior can be appreciated for the imaginary part. Moreover, the latter shows a drain current reduction with increasing temperature in all the selected operating conditions, while the real part presents the same trend in compression conditions only.

The T-dependency of the third drain harmonic as a function of the input power is shown in Fig. 7. The real part

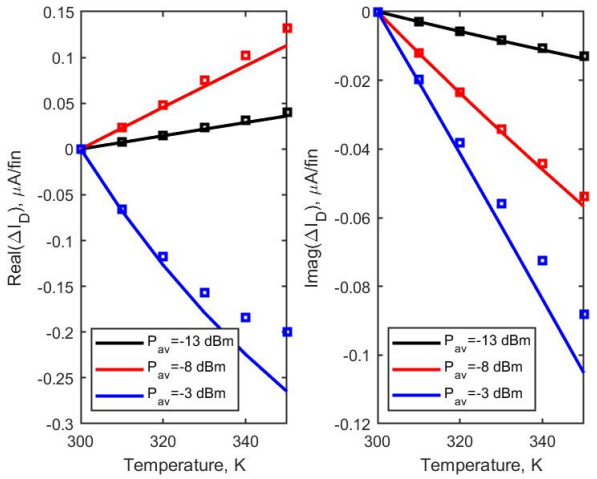

Fig. 6. Real and imaginary part of the second harmonic drain current variation as a function of temperature. Lines: INC approach. Symbols: GF approach.

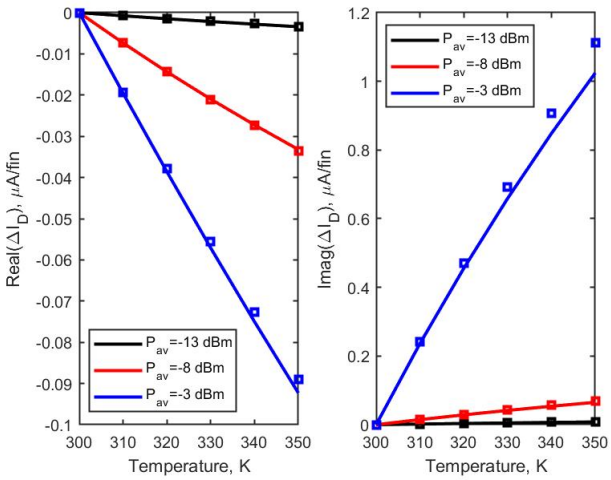

Fig. 7. Real and imaginary part of the third harmonic drain current variation as a function of temperature. Lines: INC approach. Symbols: GF approach.

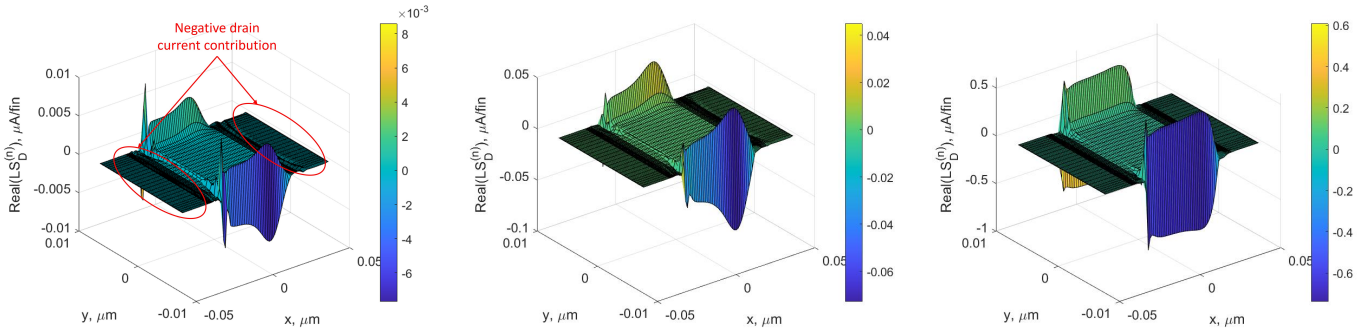

Fig. 8. Real part of the electrons distributed local sources of the third harmonic at drain contact. Left: $P_{\text{av}} = -13$ dBm. Center: $P_{\text{av}} = -8$ dBm. Right: $P_{\text{av}} = -3$ dBm.

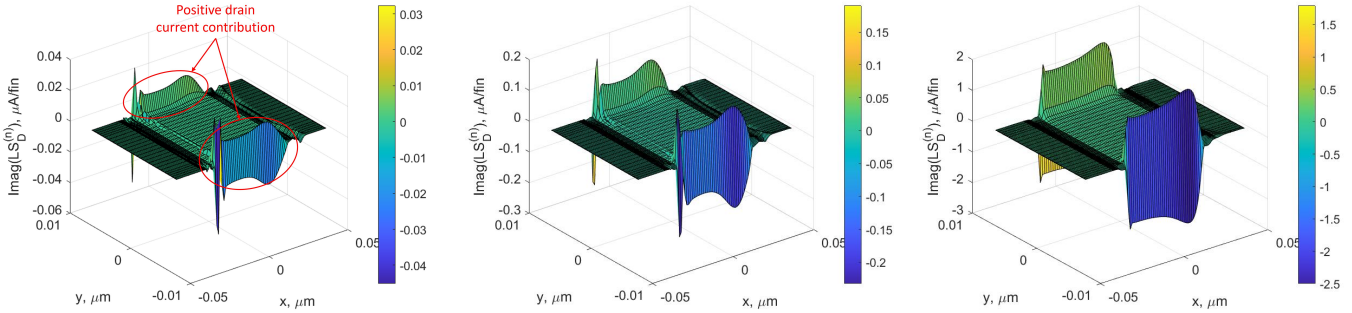

Fig. 9. Imaginary part of the electrons distributed local sources of the third harmonic at drain contact. Left: $P_{\text{av}} = -13$ dBm. Center: $P_{\text{av}} = -8$ dBm. Right: $P_{\text{av}} = -3$ dBm.

presents an opposite behavior with respect to the first and second drain harmonics: an increasing drain current variation is reported going from back-off to compression. Furthermore, the imaginary part is less sensitive to temperature variations for lower input power values and reaches the highest sensitivity in compression conditions.

In order to gain a further insight, we delve into the spatial distributions leading to the terminal current variations. Taking as an example the third harmonic, we report the electron distributed local source at the drain contact, corresponding to the electron continuity equation contribution to the total drain current variation (9)

$$\mathbf{LS}_{\text{D}}^{(n)} = \mathbf{\Omega}_{\text{V}} \tilde{\mathbf{G}}_{\text{D}}^{(n)}(\tilde{\mathbf{x}}_0, \mathbf{e}; T_0) \tilde{\mathbf{s}}^{(n)}(\tilde{\mathbf{x}}_0, \mathbf{e}; T_0, T_0 + \Delta T) \quad (10)$$

where ΔT is set to 5 K. The real part of the distributed local source confirms an increasing sensitivity going from -13 dBm to -3 dBm and shows an interplay between the bulk region and the interface between Si and oxide (see Fig. 8). The negative drain harmonic variation (see Fig. 7, left) can be traced back to the source and drain access regions, where the mobility reduction due to temperature affects the harmonics. Moreover, the strong electric field of the access regions has a further impact on the mobility degradation, which dominates over the channel T dependency. On the contrary, the imaginary part, showing a higher sensitivity to T with respect to the real part, is mostly affected by the region under the gate due to the channel charge modulation (see Fig. 9). The effect of temperature is stronger close to the oxide interface, where the influence of the exponential functions involving the electrostatic potential, rule the electron concentration in the device channel and the capacitive coupling to the gate contact. The higher electron concentration, the milder electric field in the channel region and the consequent lower mobility degradation lead to a positive drain current variation of the third harmonic.

IV. Conclusion

We presented a detailed discussion of the physical origin of temperature-induced terminal current variations for Si FinFET class A power amplifier operated at 70 GHz for transceiver applications. The unique combination of TCAD physical simulations of the device, and of a linearized, Green's Function approach to parametric perturbations in large-signal operation of the device allow for and in depth discussion on the device regions mostly affecting the T-induced current variations, and to trace them back to specific regions of the device. The numerical advantage provided by the GF approach, that was validated up to 50 K temperature increase, allows a significant efficiency improvement (simulation time reduced to about 20% of the INC approach). These results pave the way towards an optimized device design to quench self-heating effects.

Acknowledgment

This work has been supported by the Italian MIUR PRIN 2017 Project "Empowering GaN-on-SiC and GaN-on-Si

technologies for the next challenging millimeter-wave applications (GANAPP)"

REFERENCES

[1] B. Troyanovsky, Z. Yu, and R. W. Dutton, "Large signal frequency domain device analysis via the harmonic balance technique," in *Simulation of Semiconductor Devices and Processes*. Springer Vienna, 1995, pp. 114–117.

[2] F. M. Rotella, G. Ma, Z. Yu, and R. W. Dutton, "Design optimization of RF power MOSFET's using large signal analysis device simulation of matching networks," in *Simulation of Semiconductor Processes and Devices 1998*. Springer Vienna, 1998, pp. 26–29.

[3] F. Bonani, S. Donati Guerrieri, G. Ghione, and M. Pirola, "A TCAD approach to the physics-based modeling of frequency conversion and noise in semiconductor devices under large-signal forced operation," *IEEE Transactions on Electron Devices*, vol. 48, no. 5, pp. 966–977, may 2001.

[4] S. Donati Guerrieri, E. Catoggio, and F. Bonani, "TCAD simulation of microwave circuits: The Doherty amplifier," *Solid-State Electronics*, vol. 197, p. 108445, nov 2022.

[5] E. Catoggio, S. Donati Guerrieri, and F. Bonani, "Efficient TCAD thermal analysis of semiconductor devices," *IEEE Transactions on Electron Devices*, vol. 68, no. 11, pp. 5462–5468, nov 2021.

[6] S. Donati Guerrieri, F. Bonani, F. Bertazzi, and G. Ghione, "A unified approach to the sensitivity and variability physics-based modeling of semiconductor devices operated in dynamic conditions—Part I: Large-signal sensitivity," *IEEE Transactions on Electron Devices*, vol. 63, no. 3, pp. 1195–1201, mar 2016.

[7] F. Bertazzi, F. Bonani, S. Donati Guerrieri, and G. Ghione, "Physics-based SS and SSLS variability assessment of microwave devices through efficient sensitivity analysis," in *2012 Workshop on Integrated Nonlinear Microwave and Millimetre-wave Circuits*. IEEE, sep 2012.

[8] [Online]. Available: https://www.synopsys.com/silicon/tcad.html

[9] A. M. Bughio, S. Donati Guerrieri, F. Bonani, and G. Ghione, "Physics-based modeling of FinFET RF variability," in *2016 11th European Microwave Integrated Circuits Conference (EuMIC)*. IEEE, oct 2016.

[10] E. Catoggio, S. Donati Guerrieri, C. Ramella, and F. Bonani, "Thermal modeling of RF FinFET PAs through temperature-dependent X-parameters extracted from physics-based simulations," in *2022 International Workshop on Integrated Nonlinear Microwave and Millimetre-Wave Circuits (INMMiC)*. IEEE, apr 2022.

[11] K. S. Kundert, J. K. White, and A. Sangiovanni-Vincentelli, *Steady-state methods for simulating analog and microwave circuits*. Boston: Kluwer Academic Publishers, 1990.